Supporting information

Accelerating electron transfer in heterogeneous catalytic ozonation via ligand effect: A dual-pathway synergistic mechanism

Xiaojun Du[1], Haokun Bai[2], Lanlan Liang[3], Shuo Chen[1], Xie Quan (✉)[1]

1 Key Laboratory of Industrial Ecology and Environmental Engineering (Ministry of Education, China), School of Environmental Science and Technology, Dalian University of Technology Dalian, Dalian 116024, China

2 Guangdong Provincial Key Laboratory of Environmental Pollution Control and Remediation Technology, School of Environmental Science and Engineering, Sun Yat-sen University, Guangzhou 510275, China

3 Key Laboratory of Water Supply & Sewage Engineering of Ministry of Housing and Urban-rural Development, School of Civil Engineering, Chang'an University, Xi'an 710061, China

✉ Corresponding author
E-mail: quanxie@dlut.edu.cn

Text S1: ROS detection during ozonation by EPR

The types of radicals present during catalytic ozonation were verified by electron paramagnetic resonance (EPR, A200–9.5/12, Bruker, Germany) technique, using TEMP and DMPO as spin-trapping agents. To identify ·OH and carbon-centered radicals ($C_2O_4^{\bullet-}$ and $CO_2^{\bullet-}$), O_3 was continuously bubbled into the reaction system. After 5 min of reaction, a 5 mL aliquot of the suspension was withdrawn and transferred to a 10 mL centrifuge tube, followed by the immediate addition of the spin-trapping agent DMPO to quench radicals. After shaking for a period, a sample of the liquid was withdrawn using a capillary tube and then capped with paraffin for later detection. During the assay, the sample was scanned five times consecutively. For the detection of $\cdot O_2^-$, the reaction was conducted in a methanol solution. The spin-trapping agent TEMP was employed for the identification of $^1O_2$, and the other detection procedures were the same as those for ·OH and $\cdot O_2^-$.

Text S2: Fitting procedures of XPS spectra.

All binding energies were referenced to the C 1s peak at 284.6 eV, and a Shirley background was adopted for spectral fitting. The areas of spin-orbit split peaks were 3:2 for $3d_{5/2}$: $3d_{3/2}$. The calibrated Ce 3d spectra were fitted with six peaks (v, v'', v''', u, u'', u''') of Ce(IV) and two peaks (v_0, u_0) for Ce(III), with details on peak positions provided in Tables S2–S4. In the Ce $3d_{5/2}$ spin-orbit split doublet for Ce(IV), v and v''' represent the intense peaks and v'' was a weak satellite. Correspondingly, u and u''' represent the intense peaks of Ce $3d_{3/2}$ spin-orbit split doublet for Ce(IV), while u'' was the satellite. For Ce(III), v_0 was the signal of Ce $3d_{5/2}$ spin-orbit split, while u_0 represent the Ce $3d_{3/2}$ spin-orbit split. The relative content of Ce(III) on the surface can be calculated from the integrated intensity of the v_0, u_0 peaks relative to the total Ce 3d spectral area, using Equation (S1).

$$Ce(III)=\frac{v_o+u_0}{\sum(v+u)} \qquad (S1)$$

Text S3: LC-MS measurement

The degradation intermediates of IBU were identified using LC-MS in negative ESI mode. Chromatographic separation was achieved using an Eclipse C18 column (2.1 × 100 mm × 3.5 μm) with mobile phases consisting of (A) ultrapure water

containing 0.1 wt% formic acid and (B) acetonitrile. The temperature of the column was maintained at 30 °C. A flow rate of 0.25 mL/min and an injection volume of 10 μL were used. The operating conditions for the electrospray ionization source were as follows: nebulizer 25 psi; capillary 15 nA; drying gas (N_2) temperature 350 °C; drying gas flow rate 8 mL/min.

Text S4: Preparation method for the CeO_2-OA complex

To investigate the surface properties of the catalyst after interacting with the organic ligand, the CeO_2-OA complex was prepared using a batch adsorption-filtration method. Specifically, a known mass of CeO_2 powder was dispersed into an aqueous solution of oxalic acid (OA) under continuous magnetic stirring for 30 min to ensure sufficient surface coordination. Subsequently, the resulting suspension was filtered through a 0.22-μm membrane, and the recovered solid was thoroughly rinsed with deionized water multiple times to remove any physisorbed or residual OA. Finally, the CeO_2-OA complex was dried in a vacuum oven at 60 ℃ for 12 h prior to FTIR analysis.

Table S1. HPLC detection conditions of different contaminants

Chemical name	Structure	Mobile phase		Wavelength (nm)
		A	B	
IBU	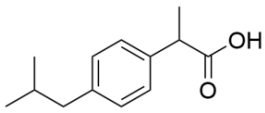	Acetonitrile 70%	Water (0.1vol.% Formic acid) 30%	223
OA	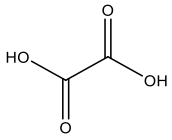	Methanol 2%	Water (2 wt% aluminium dihydrogen phosphate) 98%	197

Table S2. Fitting parameters of Ce 3d XPS spectra of sole CeO_2-catalyzed system

Symbol	Peak	Binding Energy (eV)	Valence	Atomic (%)
v	Ce $3d_{5/2}$	882.20	Ce(IV)	20.28
v''	Ce $3d_{5/2}$	888.74	Ce(IV)	9.92
v'''	Ce $3d_{5/2}$	898.11	Ce(IV)	21.48
u	Ce $3d_{3/2}$	900.64	Ce(IV)	9.87
u''	Ce $3d_{3/2}$	907.23	Ce(IV)	7.11
u'''	Ce $3d_{3/2}$	916.41	Ce(IV)	13.63
v_0	Ce $3d_{5/2}$	884.70	Ce(III)	13.64
u_0	Ce $3d_{3/2}$	902.60	Ce(III)	4.05

Table S3. Fitting parameters of Ce 3d XPS spectra of CeO_2/O_3 system

Symbol	Peak	Binding Energy (eV)	Valence	Atomic (%)
v	Ce $3d_{5/2}$	882.17	Ce(IV)	25.25
v''	Ce $3d_{5/2}$	888.79	Ce(IV)	9.55
v'''	Ce $3d_{5/2}$	898.08	Ce(IV)	21.49
u	Ce $3d_{3/2}$	900.64	Ce(IV)	8.32
u''	Ce $3d_{3/2}$	907.18	Ce(IV)	6.57
u'''	Ce $3d_{3/2}$	916.39	Ce(IV)	12.92
v_0	Ce $3d_{5/2}$	884.77	Ce(III)	10.08
u_0	Ce $3d_{3/2}$	902.64	Ce(III)	5.83

Table S4. Fitting parameters of Ce 3d XPS spectra of OA/CeO_2/O_3 system

Symbol	Peak	Binding Energy (eV)	Valence	Atomic (%)
v	Ce $3d_{5/2}$	881.90	Ce(IV)	23.66
v''	Ce $3d_{5/2}$	888.52	Ce(IV)	8.66
v'''	Ce $3d_{5/2}$	897.87	Ce(IV)	21.14
u	Ce $3d_{3/2}$	900.44	Ce(IV)	8.24
u''	Ce $3d_{3/2}$	906.83	Ce(IV)	6.58
u'''	Ce $3d_{3/2}$	916.15	Ce(IV)	12.22
v_0	Ce $3d_{5/2}$	884.76	Ce(III)	12.87
u_0	Ce $3d_{3/2}$	902.46	Ce(III)	6.63

Table S5. Intermediates of IBU degradation detected by LC-MS (ESI-).

Number	Proposed structure	Formula	ESI (-) MS, m/z	MW
	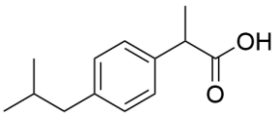	$C_{13}H_{18}O_2$	205	206
P1	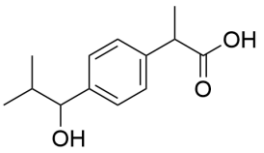	$C_{13}H_{18}O_3$	221	222
P2	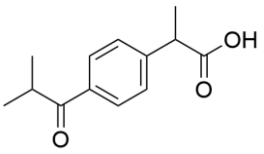	$C_{13}H_{16}O_3$	219	220
P3	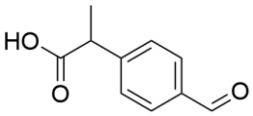	$C_{10}H_{10}O_3$	177	178
P4	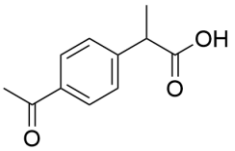	$C_{11}H_{12}O_3$	191	192
P5	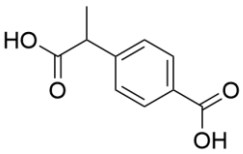	$C_{10}H_{10}O_4$	193	194
P6	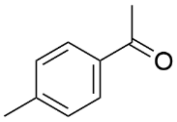	$C_9H_{10}O$	133	134
P7	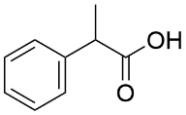	$C_9H_{10}O_2$	149	150
P8	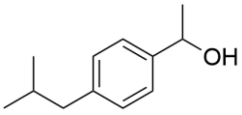	$C_{12}H_{18}O$	177	178
P9	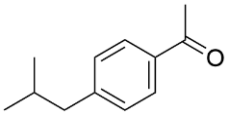	$C_{12}H_{16}O$	175	176
P10	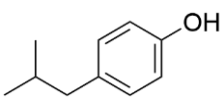	$C_{10}H_{14}O$	149	150

P11	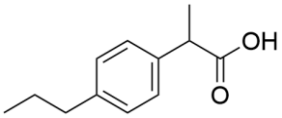	$C_{12}H_{16}O_2$	191	192
P12	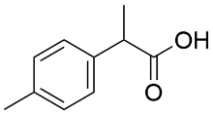	$C_{10}H_{12}O_2$	163	164
P13	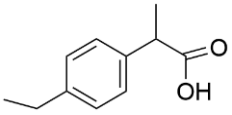	$C_{11}H_{14}O_2$	177	178
P14	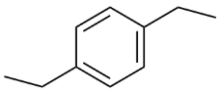	$C_{10}H_{14}$	132	133
P15	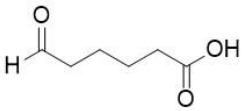	$C_6H_{10}O_3$	129	130
P16	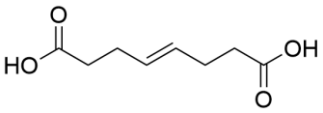	$C_8H_{12}O_4$	171	172

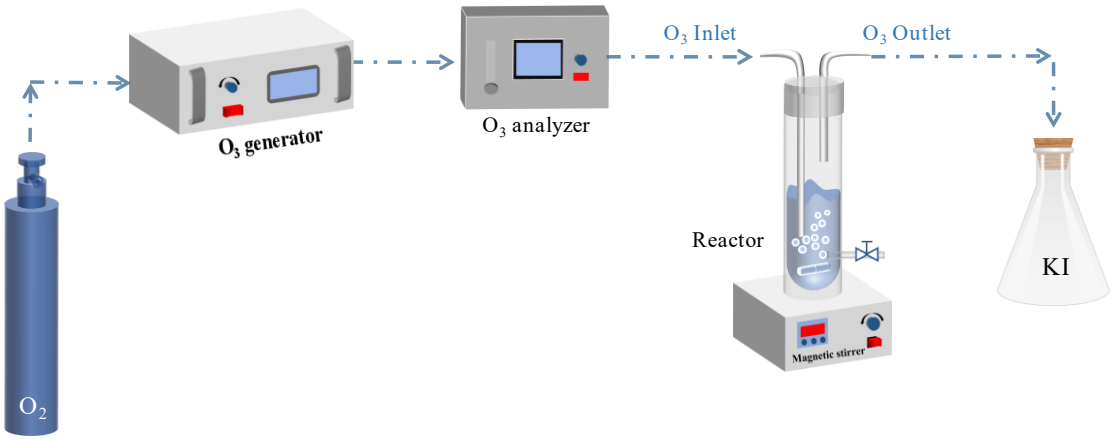

Fig. S1. Schematic diagram of catalytic ozonation reactor for experiments.

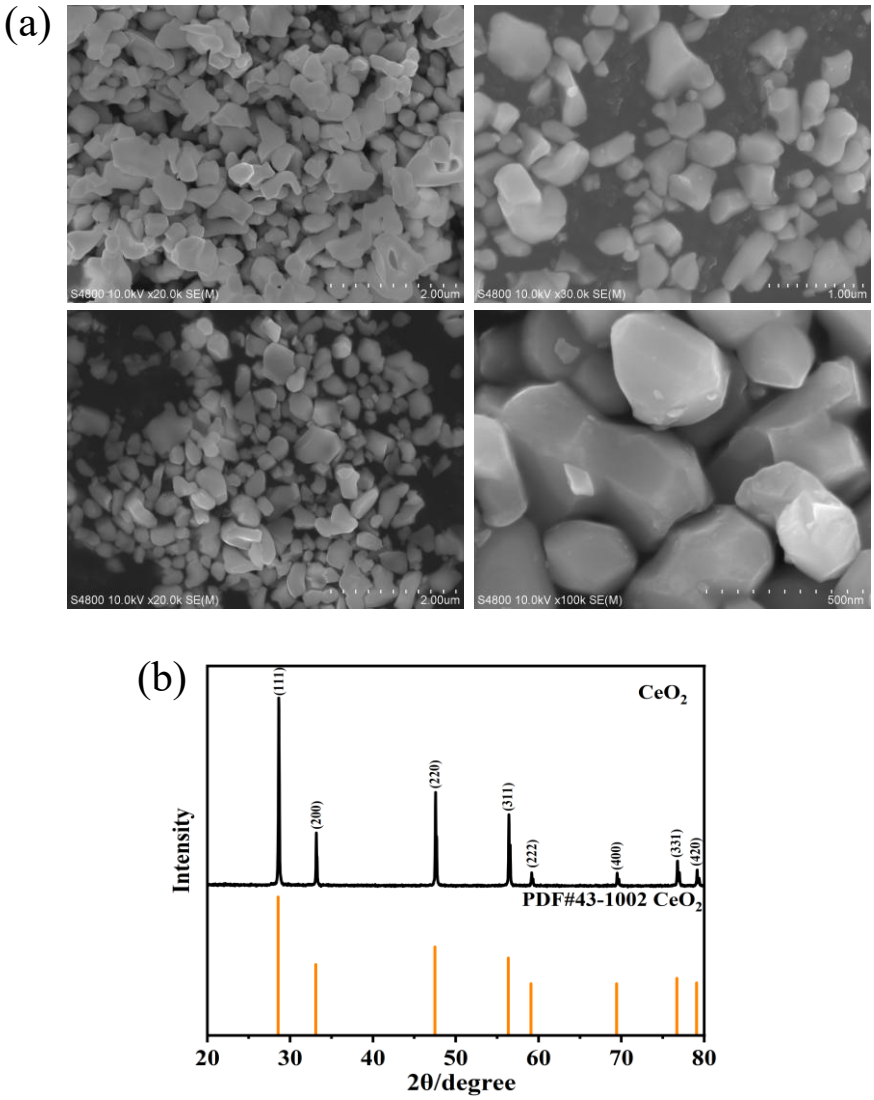

Fig. S2. (a) SEM images of CeO_2 at different magnifications;

(b) XRD pattern of CeO_2.

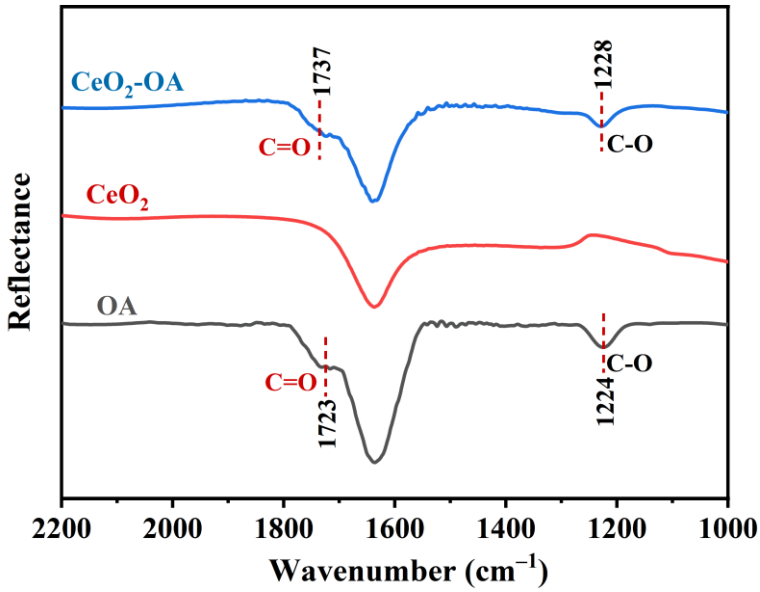

Fig. S3. ATR-FTIR spectra of CeO_2-OA, CeO_2, and OA.

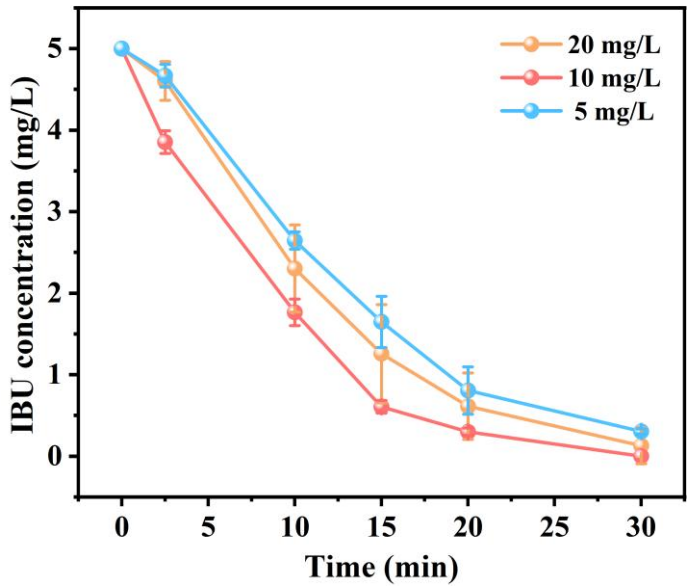

Fig. S4. Effect of ligand OA concentration on the IBU degradation efficiency of CeO_2/OA/O_3 system.

([IBU] = 5 mg/L, [OA] = 5, 10, 20 mg/L)

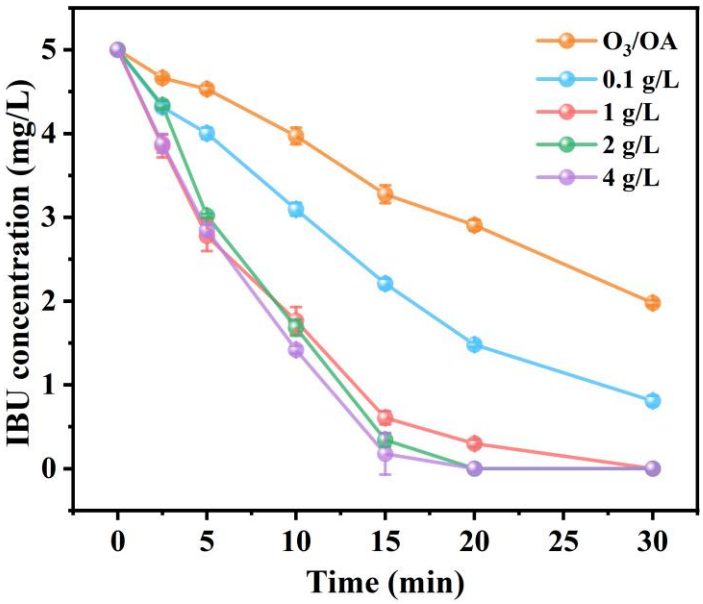

Fig. S5. Effect of catalyst dosage on the IBU degradation efficiency of CeO_2/OA/O_3 system.

([IBU] = 5 mg/L, [CeO_2] = 0.1, 1, 2, 4 mg/L)

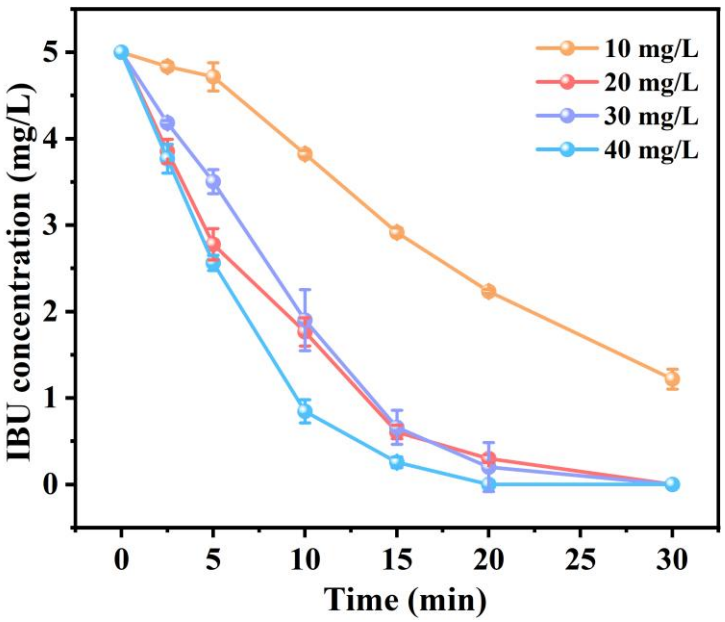

Fig. S6. Effect of ozone concentration on the IBU degradation efficiency of CeO_2/OA/O_3 system.

([IBU] = 5 mg/L, [O_3] = 10, 20, 30, 40 mg/L)

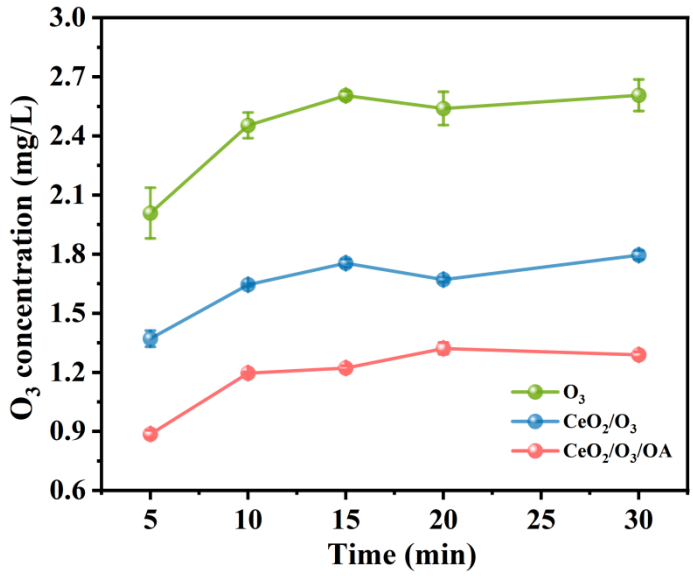

Fig. S7. Residual ozone concentration of different reaction systems.

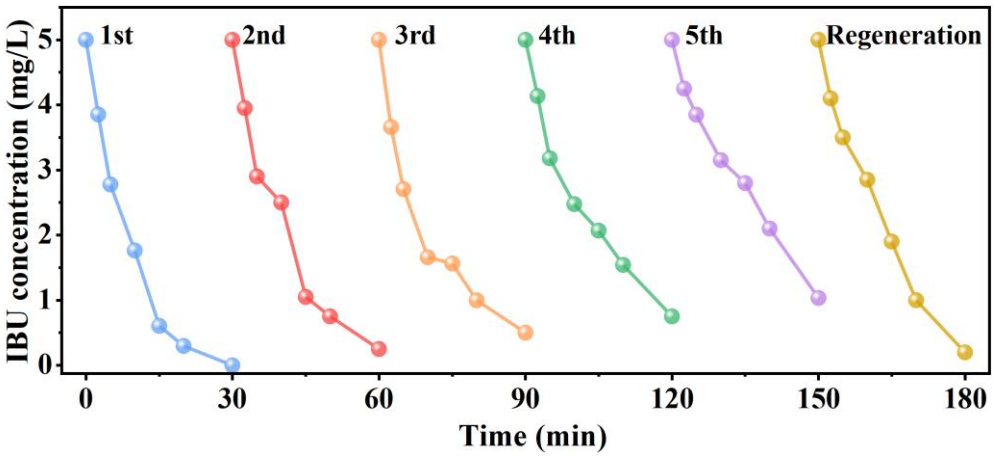

Fig. S8. Evaluation of catalytic reusability.

([IBU] = 5 mg/L; [OA] = 10 mg/L; [CeO_2] = 1.0 g/L; [O_3] = 20 mg/L; pH = 3.5)

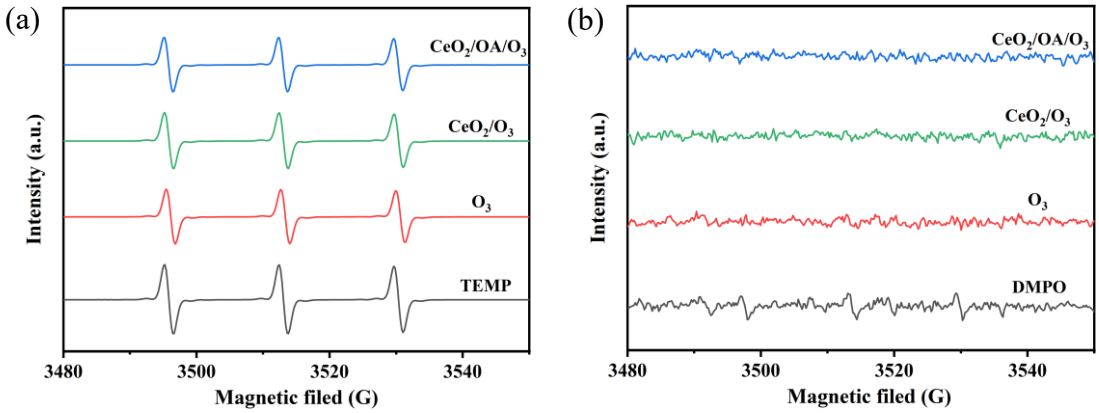

Fig. S9. (a) TEMP span-trapping EPR spectra of TEMP–$^1O_2$ in water. (b) DMPO span-trapping EPR spectra of DMPO–$O_2^{\cdot-}$ in methanol.

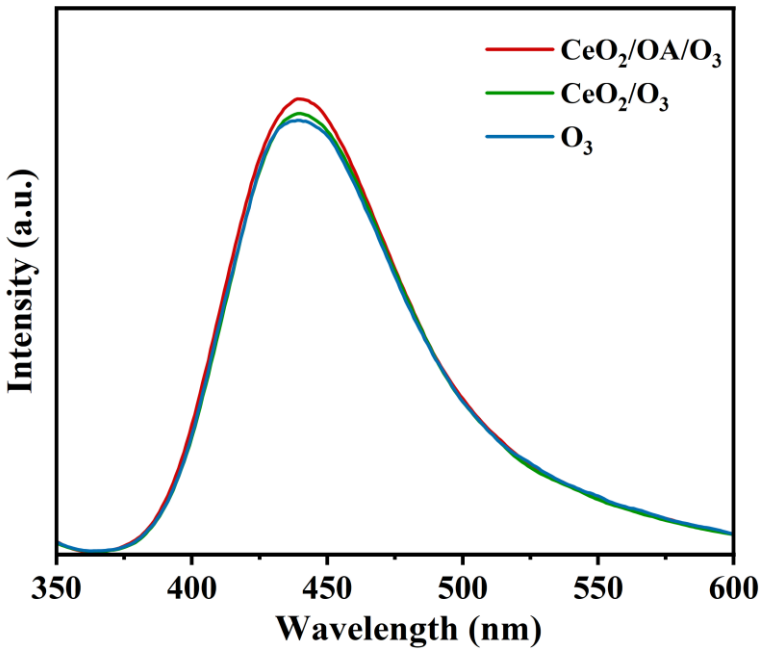

Fig. S10. Fluorescence spectroscopy for detecting ·OH in different systems.

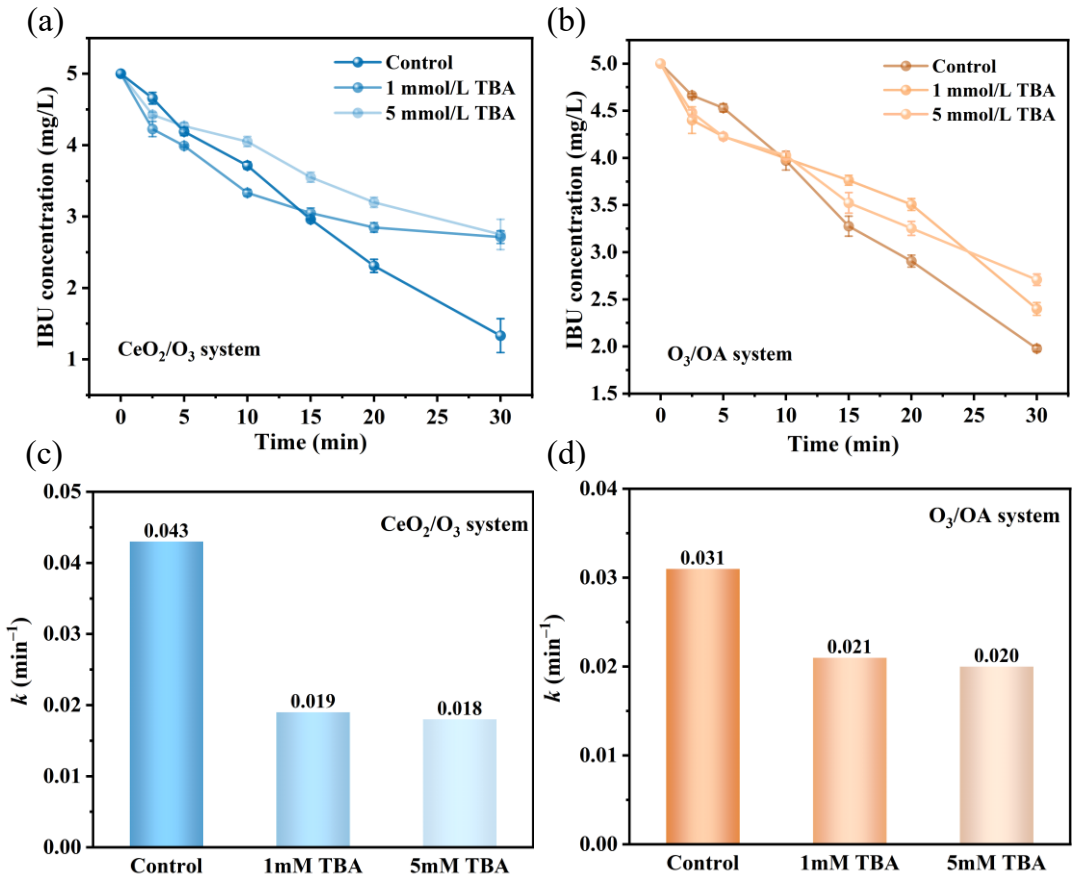

Fig. S11. (a) Effect of TBA on the catalytic performance of CeO_2/O_3 system and (c) corresponding reaction rate constants. (b) Effect of TBA on the catalytic performance of O_3/OA system and (d) corresponding reaction rate constants.

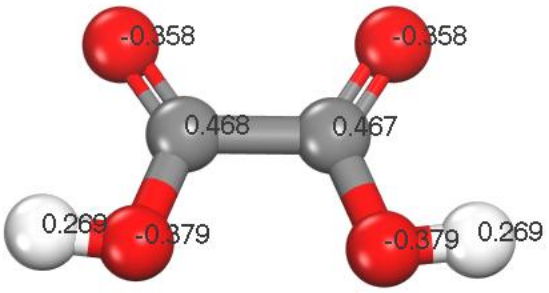

Fig. S12. The electron population number of OA.

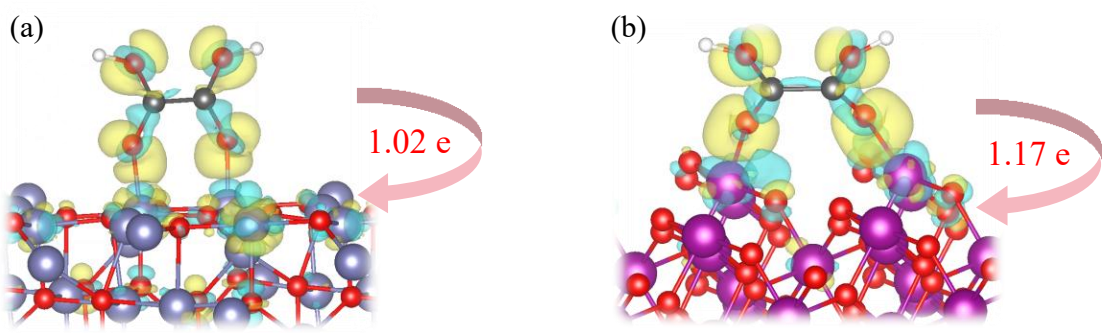

Fig. S13. Differential charge population and Bader charge analysis of (a) Fe_3O_4/OA and (b) MnO_2/OA.

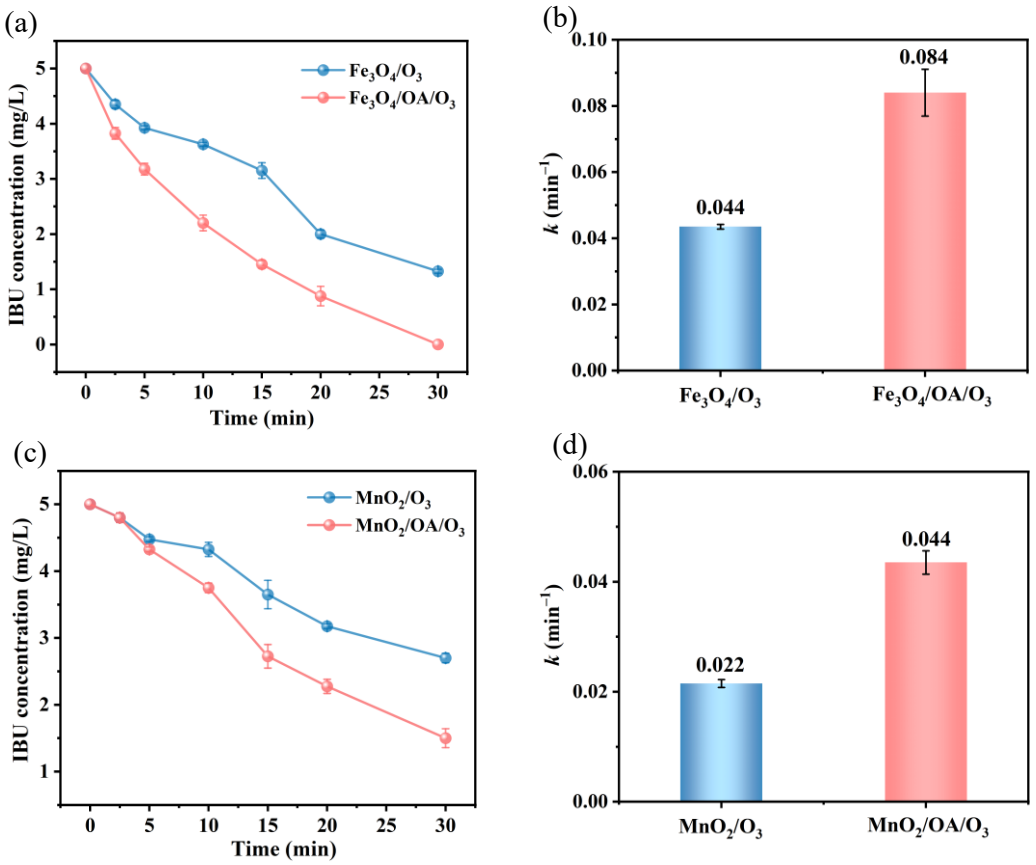

Fig. S14. Catalytic ozonation of IBU in (a) Fe_3O_4/O_3 and $Fe_3O_4/OA/O_3$ systems and (b) corresponding reaction rate constants. (c) MnO_2/O_3 and $MnO_2/OA/O_3$ systems and (d) corresponding reaction rate constants.

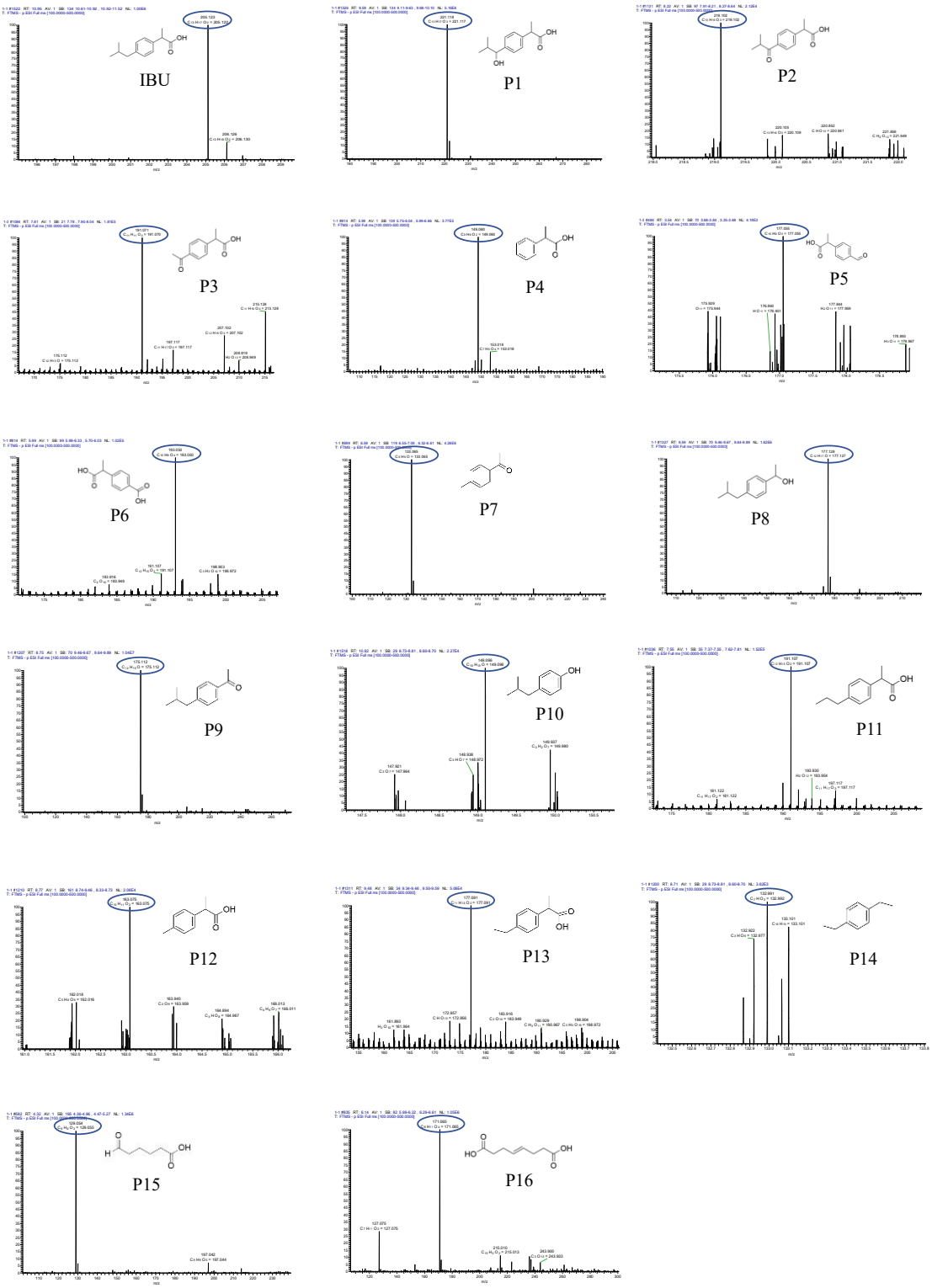

Fig. S15. The identification intermediates of P1–16 in OA/CeO_2/O_3 system.